An Inelastic Finite Element Model of 4D Carbon-Carbon Composites

L. Delneste* and B. Perez*
Société Européenne de Propulsion, Bordeaux, France

Sepcarb 4D is a carbon-carbon composite material wherein the reinforcing fibers are bundled in four directions. It is widely and successfully used in integral solid rocket nozzles. However, an accurate prediction of the material behavior is difficult, due to the anisotropy and above all to the nonlinear inelasticity of the composite. An elastoplastic finite element model, including homogenized monoaxial stiffnesses, is presented. A consistent set of constitutive constants is obtained from test data. The adequacy of the model is demonstrated through comparisons between predicted and measured test results of Sepcarb 4D uniaxial specimens and rings. Results showing the significant influence of the orientation of the 4D reinforcements relative to the applied load are discussed. The model can be extended to an increased number of directional composites and offers new possibilities in the stress analysis of such materials.

Nomenclature

B	= nodal displacements to strain matrix $\epsilon = Bu$
C	= isotropic Hooke's matrix
d	= rod direction
e	= thickness of a ring
E, E'	= Young's moduli; the direction is defined by subscripts X, Y, Z, X', and R
E_r	= Young's modulus of a carbon rod
G	= shear modulus
H	= orthotropic Hooke's matrix
h	= slope of effective stress vs effective plastic strain curve
$J1$	= first stress invariant $= \sigma_{ii}$
$J2$	= second stress deviator invariant $= SijSij/2$; $Sij = \sigma_{ij} - \delta_{ij}\sigma_{kk}/3$
k, K	= elastic monoaxial stiffness; $K = (4/9)k$
P	= external pressure applied to a ring
r	= current radius of ring
r_0	= mean radius of ring
R	= stiffness matrix defined by Eqs. (5) and (6)
s	= $\{\partial\bar{\sigma}/\partial\sigma\}$ column vector; $s^t = (\partial\bar{\sigma}/\partial\sigma_1, \partial\bar{\sigma}/\partial\sigma_2 \ldots \partial\bar{\sigma}/\partial\sigma_{23})$
T	= column vector giving a monoaxial strain from strain vector defined in Eq. (4)
t	= fiber volume fraction of rods which are oriented in a direction d_i
u	= nodal displacements column vector
V	= inner radial displacement of a ring
x, y, z	= compliances ($x = 1/E$, $y = 1/E'$, $z = 1/G$)
ϵ	= column strain vector: $\epsilon^t = (\epsilon_1, \epsilon_2, \epsilon_3, \gamma_{12}, \gamma_{23}, \gamma_{31})$
$\bar{\epsilon}^P$	= equivalent plastic strain
θ	= angle of rotation around Y' in Fig. 3 and around Z in Eq. (3)
ν	= Poisson's ratio
σ	= column stress vector
$\bar{\sigma}$	= equivalent von Mises stress $= (1/\sqrt{2})[(\sigma_1 - \sigma_2)^2 + (\sigma_2 - \sigma_3)^2 + (\sigma_3 - \sigma_1)^2 + 6(\sigma_{12}^2 + \sigma_{23}^2 + \sigma_{31}^2)]^{1/2}$

Superscript and Subscripts

T	= vector or matrix transposition
i	= index of a rod direction = 1-4
is	= isotropic constituent
X, Y, Z, X', Y'	= Cartesian coordinates defined in Fig. 1.

Presented as Paper 81-1463 at the AIAA/SAE/ASME 17th Joint Propulsion Conference, Colorado Springs, Colo., July 27-29, 1981; submitted Aug. 12, 1981; revision received Sept. 14, 1982.

*Research Engineer, Research Department.

I. Introduction

THE 4D (four-direction) carbon-carbon composite[1,2] is a particularly attractive material for use in advanced solid rockets, and arouses the interest of nosetip designers. It is now widely used because of its suitable thermomechanical properties in the design of nozzle components such as the integral throat entrance (ITE), which is subjected to a severe environment in firing.

Several studies[3-5] have been conducted for the purpose of modeling the macroscopic behavior of such directional reinforced C-C composites with respect to their actual anisotropy. Preliminary investigations on specimens and full-scale 4D components indicate, however, that nonlinear inelasticity is often its most significant behavior characteristic. Therefore, a suitable choice of the 4D texture orientation and an accurate prediction of the behavior of the composite require computational analyses that account for both the anisotropy and the inelasticity of the material.

The purposes of this paper are to: 1) summarize the principal test results about 4D anisotropy, both for elastic and inelastic fields, 2) present an elastoplastic three-dimensional finite element model for 4D structural analysis, 3) compare predicted and measured results of specimen and ring tests, and 4) introduce the 4D failure analysis capabilities of the model.

II. Geometric Properties and Test Data

A. Geometry

The 4D configuration is obtained from the regular interlacing of rectilinear thread bundles wherein the four directions of rods are defined by the directions of the four long diagonals of a cube, as shown in Fig. 1. Hence the thread bundles also form perpendiculars to the four sides of a regular tetrahedron. In the material of interest, the bundles are 1-mm-diam carbon rods and the fiber volume fraction is 0.68. The remaining volume, i.e., 32% of the composite volume, constitutes an open macroporosity enabling an efficient densification using pitch impregnation and isostatic pressure carbonization.

The definition of the reference axes is shown in Fig. 1. The X, Y, and Z axes are perpendicular to the cube faces. The X' and Y' axes are in the same plane as the X and Y axes but are rotated through 45 deg about the Z axis.

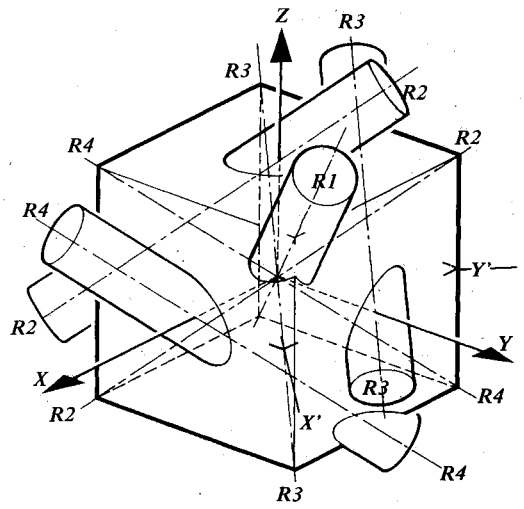

Fig. 1 Geometry of the 4D texture.

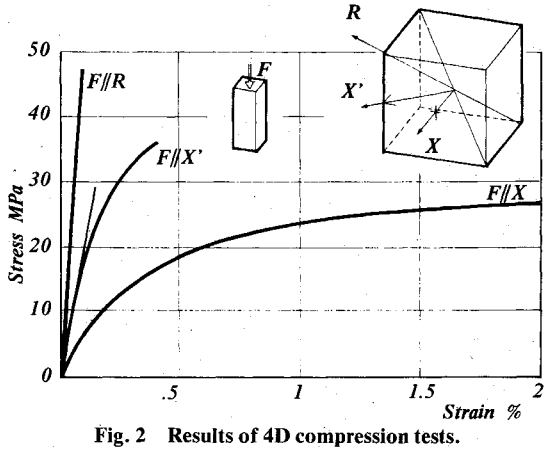

Fig. 2 Results of 4D compression tests.

B. Mechanical Behavior Obtained from Specimen Test Data

Results of compression tests of specimens are used to investigate the behavior of the 4D composite in different directions relative to the rod orientations. Compression tests are performed on square section bars ($19\times19\times46$ mm). The length axis of the bars, which is also the direction of loading, is oriented in a chosen direction relative to the orientation of the reinforcements.

Figure 2 is the stress-strain response obtained according to the three directions of loading X, X', and R (these monoaxial compression tests are termed, respectively the X, X', and R tests). These curves show the anisotropy of the 4D material and exhibit the nonlinear behavior for X and X' tests and linear behavior for the R test. For very small strains ($\epsilon<0.1\%$), the material behavior is linear in all directions. In this strain region, the 4D material appears to be orthotropic with three equivalent directions X, Y, Z and completely defined by constants E ($E=E_X=E_Y=E_Z$), ν ($\nu=\nu_{XY}=\nu_{YZ}=\nu_{ZX}$), and G ($G=G_{XY}=G_{YZ}=G_{ZX}$). Two other mechanical parameters are still of interest: the Young's modulus E' in an X' or Y' direction (again due to symmetry, $E'=E_{X'}=E_{Y'}$) and the Young's modulus E_R in a direction R of rods. The measured values of these elastic constants are

$$E=8.0\,\text{GPa},\quad E'=21.0\,\text{GPa},\quad E_R=45.5\,\text{GPa},\quad \nu=0.488$$

Figure 3 is in polar coordinates the angular variation of the Young's modulus and of the Poisson's ratio in a diagonal plane of the 4D reference cube (containing two rod directions) as an example of the orthotropy of the composite. On the contrary, the 4D behaves quasi-axisymmetrically around an R direction (see the Appendix).

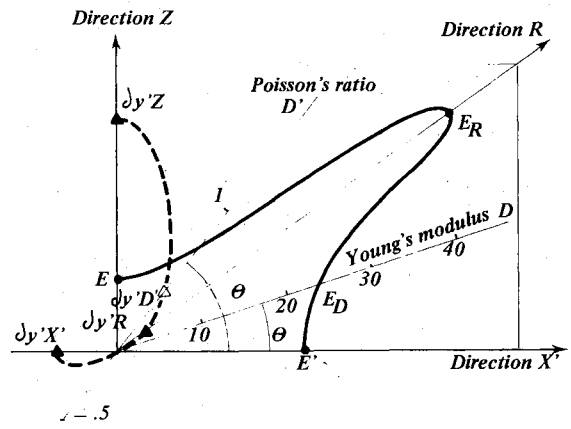

Fig. 3 Angular variation of 4D modulus and Poisson's ratio.

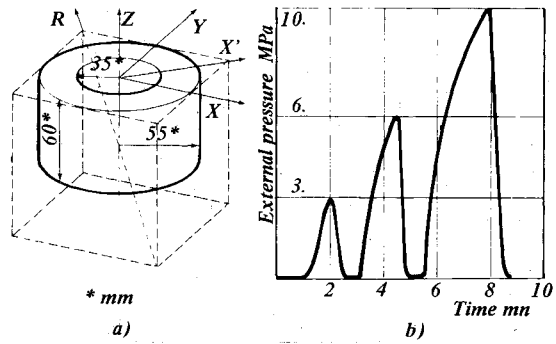

Fig. 4 4D-ring experimental definition.

The classical rotations for the transformation of the orthotropic Hooke's matrix of the 4D material from the XYZ coordinate system to systems where X' and R are first coordinate directions, respectively, yield

$$4/E'-3/E_R=1/E \tag{1}$$

$$\nu=1+2E[(1/4G)-(1/E')] \tag{2}$$

The foregoing values of E, E', and E_R are in good agreement with Eq. (1), confirming the linear elastic orthotropy of the 4D for small strains. The relation is nevertheless no longer satisfied for strains greater than 0.1%.

C. Behavior of 4D Rings Subjected to External Pressure

A geometric definition of the test rings is shown in Fig. 4a, and the applied loading as a function of time is shown in Fig. 4b. The axis of the rings coincides with the Z direction of the 4D texture. Inner radial displacements and axial displacements are measured in several angular directions, particularly in the X and X' directions. As an example, Fig. 5 is the variation of the inner radial displacement measured in the X direction during pressurization. The most significant result is the inelasticity of the material. It must be noted that when the pressure is reduced to zero the radial displacement returns linearly to a residual value along approximately parallel lines to the rectilinear portion of the initial displacement curve. Such behavior is characteristic of an elastoplasticity phenomenon.

A second significant result is obtained from the ring experiments. The inner radial displacements of the 4D ring are

$$V=A+B\cos 4\theta \tag{3}$$

with

$$A=\frac{Pr_0^2}{2e}\left(2y-\frac{z}{2}\right)\frac{r}{r_0}+\left(x-y+\frac{z}{2}\right)\frac{r_0}{r}$$

and

$$B=\frac{Pr_0^2}{60e}\frac{x-y}{x+y}(6x+10y-z)\frac{r_0}{r}-(24x+20y+z)\frac{r}{r_0}$$

Experimental data are in reasonable agreement with Eq. (3) in the low-pressure range ($P<1$ MPa). Such an agreement further confirms the assumption of linear elastic orthotropy and emphasizes that the values of the parameters obtained from specimen tests are suitable for analyses of full-scale components.

III. An Elastoplastic Finite Element Model

A. Theoretical Developments

An appropriate elastoplastic model particular to the 4D configuration and accounting for the foregoing material properties is developed. In this approach, the 4D C-C composite is mathematically represented by the superposition of the idealized 4D constituents: 1) an isotropic elastoplastic material and 2) an orthotropic elastic linear material, obtained from a homogenization of four elastic stiffnesses conveniently oriented according to the 4D rod directions.

1. Isotropic Constituent

The constitutive model is based upon the theory of isotropic elastoplasticity with a Von Mises criterion and isotropic strain hardening. Finite element computations are performed using a classical incremental scheme based upon Prandtl-Reuss equations. The stress vector increment is deduced from the total strain increment using a matrix $\boldsymbol{D}$: $\Delta\boldsymbol{\sigma}=\boldsymbol{D}\Delta\boldsymbol{\epsilon}$; this matrix $\boldsymbol{D}$ is either the Hooke's matrix $\boldsymbol{C}$ when the material is unloaded or elastically loaded, or

$$\boldsymbol{D}=\boldsymbol{C}-[\boldsymbol{C}\boldsymbol{s}\boldsymbol{s}^T\boldsymbol{C}/(h+\boldsymbol{s}^T\boldsymbol{C}\boldsymbol{s})]$$

when the material is loaded into the plastic range (more details are given in Ref. 6).

The computational analysis requires the following data: 1) the two parameters E_{is}, ν_{is} governing the elastic behavior, and 2) the work-hardening curve of this isotropic constituent, based on a plot of the stress vs plastic strain curve from the compression test.

2. Orthotropic Constituent

This material is built from the idea that each rod of the 4D texture behaves as an elastic, linear, monoaxial stiffener. The following developments are made with reference to the XYZ system of coordinates, wherein the monoaxial strain ϵ_i in a rod direction d_i is deduced from the usual complete local strain vector using a transformation vector $\boldsymbol{T}_i$. The transformation vectors can be expressed as

$$\begin{aligned}\boldsymbol{T}_i^T &= \tfrac{1}{3}(1\ \ 1\ \ 1\ \ 1\ -1\ -1), \quad i=1\\ &= \tfrac{1}{3}(1\ \ 1\ \ 1\ \ 1\ \ 1\ \ 1), \quad i=2\\ &= \tfrac{1}{3}(1\ \ 1\ \ 1\ -1\ -1\ \ 1), \quad i=3\\ &= \tfrac{1}{3}(1\ \ 1\ \ 1\ -1\ \ 1\ -1), \quad i=4\end{aligned} \tag{4}$$

and yield

$$\epsilon_i=\boldsymbol{T}_i^T\boldsymbol{\epsilon} \tag{5}$$

The assumption of linear monoaxial stiffness is expressed noting that in each direction, d_i, the monoaxial stress is proportional to the monoaxial strain:

$$\sigma_i=k\epsilon_i \tag{6}$$

giving the local strain energy density $k\boldsymbol{\epsilon}_i^T\boldsymbol{\epsilon}_i$ or $k\boldsymbol{\epsilon}^T\boldsymbol{T}_i\boldsymbol{T}_i^T\boldsymbol{\epsilon}$.

In a finite element environment, the stiffness matrix of the "homogenized material" equivalent to a rod direction can then be computed as

$$\boldsymbol{R}_i=\int_V k\boldsymbol{B}^T\boldsymbol{T}_i\boldsymbol{T}_i^T\boldsymbol{B}\mathrm{d}V \tag{7}$$

In Eq. (7) a rod of direction d_i is implicitly assumed to pass through each point of the space; this assumption can be considered as an homogenization of the rod network. By superposition of the four rod directions, the stiffness matrix modeling the global rod network is

$$\boldsymbol{R}=\sum_{i=1}^{4}\boldsymbol{R}_i=k\int_V\boldsymbol{B}^T\left(\sum_{i=1}^{4}\boldsymbol{T}_i\boldsymbol{T}_i^T\right)\boldsymbol{B}\mathrm{d}V \tag{8}$$

The comparison of Eq. (8) with the classical expression of the stiffness matrix $\boldsymbol{R}$ of an elastic material defined by a Hooke matrix $\boldsymbol{H}$

$$\boldsymbol{R}=\int_V\boldsymbol{B}^T\boldsymbol{H}\boldsymbol{B}\mathrm{d}V$$

shows that the homogenized rod network is equivalent to a material defined by a Hooke matrix

$$\boldsymbol{H}=k\sum_{i=1}^{4}\boldsymbol{T}_i\boldsymbol{T}_i^T$$

This matrix $\boldsymbol{H}$ is given using Eq. (4), in the XYZ system of coordinates, as

$$\boldsymbol{H}=\frac{4}{9}k\begin{bmatrix}1&1&1&0&0&0\\1&1&1&0&0&0\\1&1&1&0&0&0\\0&0&0&1&0&0\\0&0&0&0&1&0\\0&0&0&0&0&1\end{bmatrix}$$

This matrix $\boldsymbol{H}$ appears as the Hooke's matrix of an orthotropic material; consequently the provided superposition (isotropic plus orthotropic) will model the behavior of an orthotropic material in the range of elastic strains.

B. Finite Element Implementation

The preceding three-dimensional model defining the material behavior is used in the incremental finite element code MARC. The incremental strain to incremental stress elastic-plastic matrix $\boldsymbol{D}$ of the isotropic constituent is added to the $\boldsymbol{H}$ matrix of the orthotropic constituent. Two isoparametric elements are available: an 8-node linear brick and a 20-node quadratic brick. A preferred orientation is supplied by input of a transformation matrix, defining the XYZ characteristic directions of the 4D relative to the Cartesian system of coordinates to which the finite element grid of the component is referred.

C. Numerical Determination of Parameters

The parameters E_{is}, ν_{is}, and K must be evaluated. In addition, the work-hardening curve of the isotropic constituent, i.e., the effective stress vs effective plastic strain curve $\bar{\sigma}=f(\bar{\varepsilon}^p)$, must be supplied.

The parameters E_{is}, ν_{is}, and K are easily determined by comparing the isotropic plus orthotropic matrix of the model with the experimental orthotropic matrix obtained from the linear portion of the experimental stress-strain curves. As demonstrated in Sec. II, this experimental orthotropic Hooke matrix depends upon three constants (E,E',ν, for instance). From the definitions:

$$a=\frac{E(1-\nu)}{(1+\nu)(1-2\nu)} \qquad b=\frac{E\nu}{(1+\nu)(1-2\nu)}$$

the parameters E_{is}, ν_{is}, and K are obtained as the solution of the system

$$\frac{E_{is}(1-\nu_{is})}{(1+\nu_{is})(1-2\nu_{is})}+K=a$$

$$\frac{E_{is}\nu_{is}}{(1+\nu_{is})(1-2\nu_{is})}+K=b$$

$$\frac{E_{is}}{2(1+\nu_{is})}+K=G$$

where G can be replaced as a function of ν and E' using Eq. (2). The solution is

$$K=G-(a-b)/2 \tag{9}$$

$$E_{is}=\tfrac{1}{4}[(a-b)/(a-G)](5a+b-6G) \tag{10}$$

$$\nu_{is}=\tfrac{1}{4}(a+b-2G)/(a-G)$$

giving numerically, $K=13.312$ GPa, $E_{is}=7.991$ GPa, $\nu_{is}=0.4865$.

The value of E_{is} is therefore very close to the value of E (8 GPa). This result is due to the fact that, according to Eq. (10), $E_{is}\to E$ as $\nu\to 0.5$. The value $\nu\simeq 0.5$ is itself general for the 4D C-C composites, i.e., almost independant of material density and rods diameter, and expresses the quasi-incompressiblity of the material for small strains. The determination of the equivalent stress vs plastic strain curve of the isotropic constituent presents the prime problem, because this material is a mathematical construction without physical significance. But, because $E_{is}\simeq E$ below the yield stress, the monoaxial compression curve of the 4D in the X direction (X test; see Fig. 2) is used directly to provide both the yield stress and the work-hardening curve of the isotropic constituent.

The value of the parameter K can also be obtained by other considerations. In the material of interest, the fiber volume fraction of rods which are oriented in a given direction is $t=\pi\sqrt{3}/32$, i.e., $t=0.68/4$ from Sec. II.A. Because of the homogenization, the stiffness k should be connected to Young's modulus E_r of the rods by the relation $k=tE_r$, or $E_r=72K/\pi\sqrt{3}$. The value obtained with $K=13.312$ GPa is $E_r=176$ GPa and is in a reasonable agreement with the assumed value $E_r=200$ GPa. Reciprocally, the value of K can be obtained from the measurement of E_r and the value of t. This last procedure allows the extension of the model for materials whose reinforcing directions are not equivalent ($k_i=t_iE_{ri}$). Direct identification of K using Eq. (9) still appears to be the best way of characterization because the evaluation of E_r is difficult (modulus of the rods after composite densification).

IV. Numerical Applications

A. Analyses of 4D Specimens

Computations are first made on the compression specimens introduced in Sec. II. The $19\times19\times46$ mm bar is modeled by 12 elements (8-node bricks). The results obtained using the model defined in Sec. III are presented in Fig. 6. A good correlation is shown between calculated and measured results. With respect to the compression test in the X direction, the correlation is not trivial, but confirms the validity of the use of X tests for an accurate determination of the plastic constants. Finally, the model is in agreement with the quasi-linearity of the 4D behavior when the composite is loaded in the R direction.

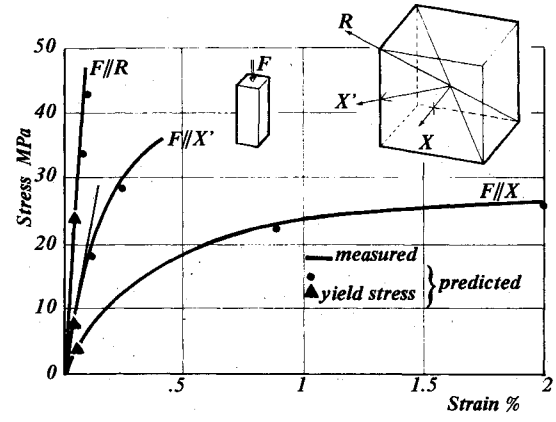

Fig. 6 Compression tests; comparison between predictions and measurements.

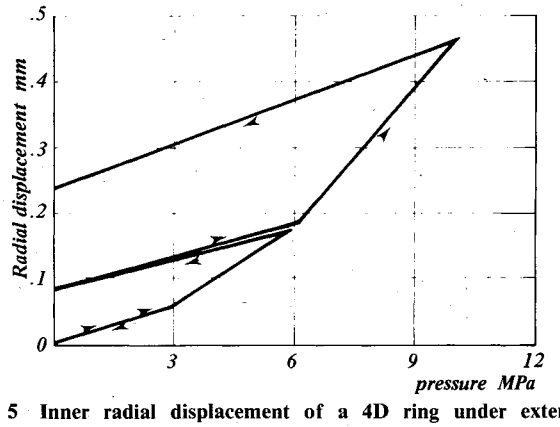

Fig. 5 Inner radial displacement of a 4D ring under external pressure.

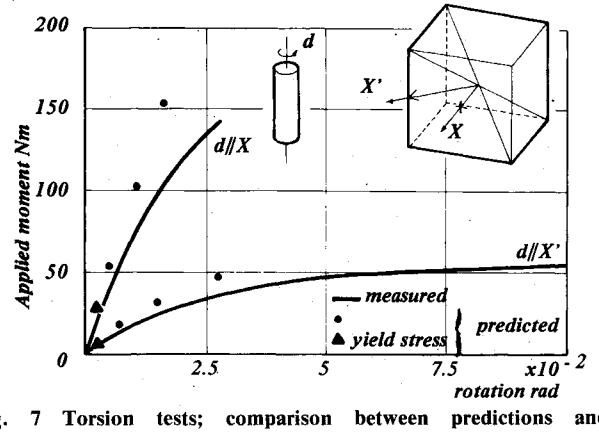

Fig. 7 Torsion tests; comparison between predictions and measurements.

The next analyses concern torsion experiments which are conducted on cylindrical specimens of 25 mm diameter and 83 mm height. The lower base of the cylinder is fixed, and the torsion is applied around the vertical axis whose orientation is chosen relative to the rod directions. Two orientations X and X' of the axis of the specimens are considered. The variation of the angle of rotation between two parallel planes 55 mm apart as a function of the applied torsional moment is shown in Fig. 7, wherein the experimental and numerical results which are obtained using a grid of 16 elements (20-node bricks) are plotted. The discrepancies between predicted and measured results are greater than those obtained for the compression tests. However, both analysis and experiment emphasize the very low yield stress and stiffness of the 4D material loaded in torsion about its X' axis. Further, Fig. 7 shows that the homogenized model overestimates the 4D torsional stiffness. More precisely, the experimental small strain shear modulus G which is calculated using the slope near the origin of the X axis torsion curve is $G=12.9$ GPa. From Eq. (2), the corresponding value in the model is $G=16$ GPa.

This discrepancy can be attributed to the influence of the specimen size on the measured value of G, as indicated by tests on specimens of increasing size from which the following mean values are obtained: $G=9.69$ GPa for 15-mm-diam, 50-mm-long cylinders; and $G=11.72$ GPa for 20-mm-diam, 60-mm-long cylinders.

Contrary to the Young's moduli, the measured shear moduli appear to be specimen size dependent. Furthermore, the necessary inequality $-1<\nu\leq 0.5$ yields, with Eqs. (1) and (2), $3G>E_R$; i.e., $G>15.27$ GPa. These results indicate that measured values of G obtained from specimens are not representative of the stiffness that would occur in a full-scale component.

B. Analyses of 4D Rings Subjected to External Pressure

The rings presented in Sec. II are analyzed using the mathematical model defined in Sec. III. Two configurations are tested and analyzed: 1) the X direction of the 4D is oriented along the axis of the ring (X ring); 2) the R direction of the material coincides with the axis of the ring (R ring).

As a consequence of the symmetry of the X ring, only a quarter-ring is modeled using 48 elements (8-node bricks). Coordinate references, displacement measurement locations, and external pressure increments are shown in Fig. 8. The predicted and the measured inner radial displacements at locations $G0$ and $G1$ (directions X and X', respectively) are plotted vs pressure in Fig. 9. The radial deformations of the inner face of the ring indicate that its form does not remain a circle but resembles an oblate square as is also demonstrated analytically [see Eq. (3)]. However, the axial displacements do not depend on the directions in the $X'Y'$ plane. Figure 9 is a good correlation between predicted and measured loading results. Nevertheless, the slopes of the return straight lines to zero pressure are underestimated (stiffness overvalued) relative to the measured results.

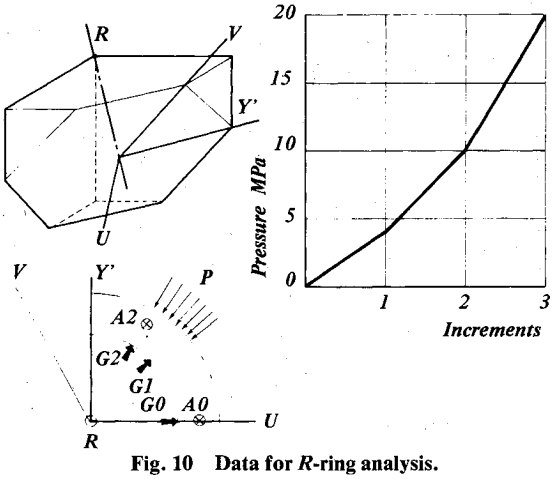

Fig. 10 Data for R-ring analysis.

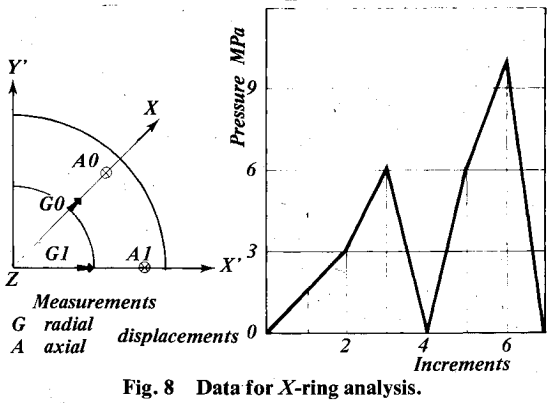

Fig. 8 Data for X-ring analysis.

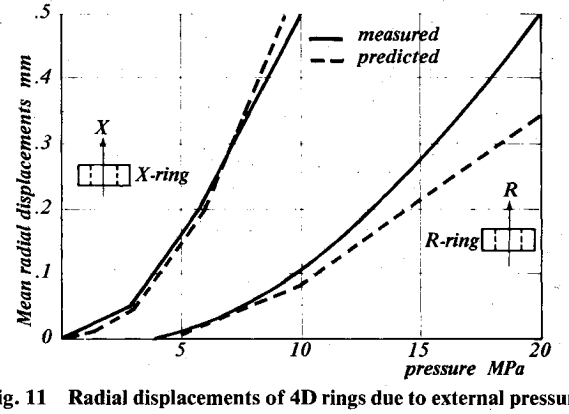

Fig. 11 Radial displacements of 4D rings due to external pressure.

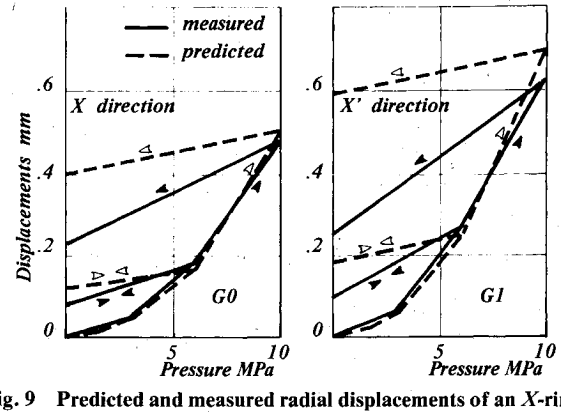

Fig. 9 Predicted and measured radial displacements of an X-ring.

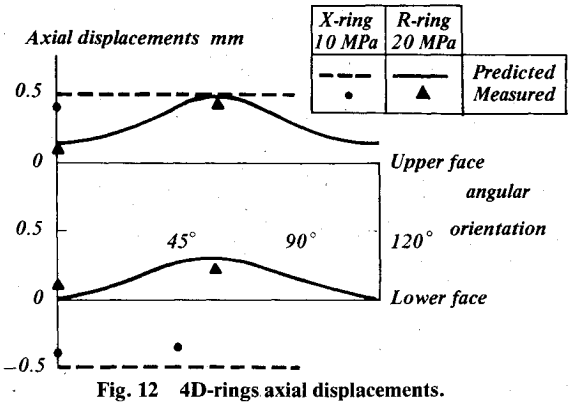

Fig. 12 4D-rings axial displacements.

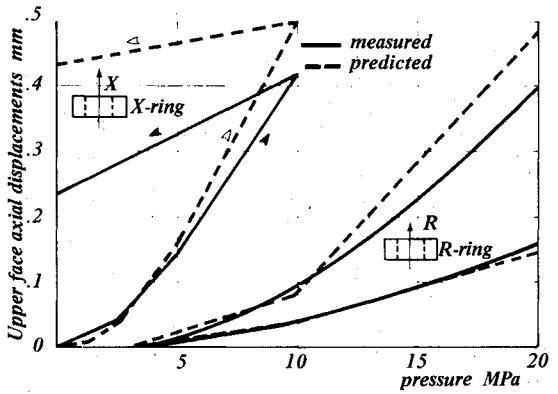

Fig. 13 Comparison between X- and R-ring axial displacements.

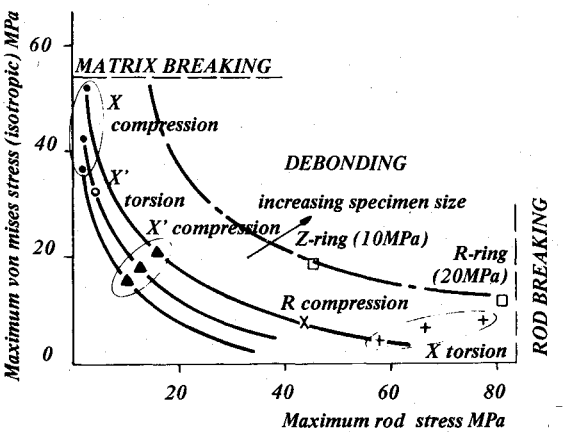

Fig. 14 4D failure diagram.

For the R-ring studies, again owing to the symmetry of this configuration, only a third of the ring needs be modeled using 48 elements (8-node bricks). Coordinate references, displacement transducer locations, and external pressure increments are shown in Fig. 10. The radial deformations of the inner face of the ring indicate that it remains approximately a circle, because of the quasi-axisymmetry of the 4D around an R axis (see Appendix). Hence only the radial displacements at the $G1$ location are compared with the mean radial displacements of the X ring, as shown in Fig. 11, where correlation between predicted and measured results is acceptable. The displacement levels are much smaller for the R ring than for the X ring. The R ring axial displacements have periodic angular variations, as shown in Fig. 12. In this figure, the displacements are not plotted at the same pressure in the two configurations because the X-ring test was stopped at 10 MPa, and the displacements of the R ring were too small at this pressure to make reasonable analysis. Figure 12 indicates a uniform expansion of the X ring, whereas the axial displacements occur in the same direction in the R-ring configuration, resulting in almost no expansion. A comparison between the predicted and the measured axial displacements of the upper face of the rings in the two configurations is shown in Fig. 13. The R-ring axial and radial displacements (Figs. 12 and 14) remain very small (less than 10^{-2} mm) up to a 4 MPa pressure; according to the computations, this pressure corresponds to the yield stress of the 4D material.

V. Further Developments

The model can be considered as a starting point for further investigations on directional C-C reinforced composites. The first application is the failure analysis of the 4D material. Two significant problems are encountered in the 4D failure investigation: 1) the definition of the failure itself and 2) the effect of specimen dimensions.

The survey of 4D specimen or ring fractures shows that the primary failure mode is a debonding of the composite between the rods and the carbon matrix; the ultimate strength (rod breaking) is then obtained for much higher strains (sometimes up to 15%). After debonding, the 4D model is no longer of use. The second difficulty indicated by the tests is that of specimen dimensions: increasing dimensions increase the specimen strength. This result is a consequence of the debonding being a function of the length of the rods in the specimen. A stress analysis is made directly using the capabilities of the model, which allows the computation of 1) the maximum equivalent Von Mises stress σ_e in the isotropic constituent and 2) the maximum monoaxial stress σ_R in the homogenized material equivalent to a rod direction using Eqs. (4-6), both at the load level corresponding to the first experimental debonding. Results are presented in Fig. 14 in the σ_R/σ_e diagram for the compression and torsion specimens according to their size. This figure also notes the results obtained for the X- and R-ring analyses, at applied pressures of 10 and 20 MPa, respectively (the failure has not been reached in the ring tests). Figure 14 shows the effect of specimen size and, qualitatively, the existence of three possible failure modes: 1) debonding, 2) matrix breaking, and 3) rod breaking. Further experiments and analyses of industrial-size components must be performed to conduct failure prediction studies.

Improvements of the model are also suggested by the comparison of computational results and experimental data, and by the known physical behavior of carbon-carbon materials. Although the model provides satisfactory results even in the inelastic behavior range, three improvements are still required.

1) The plastic behavior of C-C materials is due to matrix damage which affects its elastic properties. Consequently the parameter E_{is} should be defined as a function of damage (e.g., a linear function of $\bar{\epsilon}^p$) to reduce the discrepancies which appear during unloading between calculations and experiment.

2) The important tension vs compression behavior differences characteristic of C-C materials must be introduced in the model. This characteristic can be incorporated by considering the model constituents as bimodulus materials.[7] Such a modification can be easily applied to the rods in consequence of the hypothesis of monoxial linearity and owing to the incremental-iterative computational scheme. Equation (6) is replaced by

$$\sigma_i = k^+ \epsilon_i \quad \text{if} \quad \epsilon_i \geq 0$$

or

$$\sigma_i = k^- \epsilon_i \quad \text{if} \quad \epsilon_i < 0$$

wherein the parameters k^+ and k^- are the tension and compression stiffnesses, respectively. A similar improvement of the stress-strain law of the isotropic constituent appears to be more difficult, owing to the associated plasticity, and requires additional effort.

3) The Von Mises isotropic hardening is used for simplicity to demonstrate the accuracy of the model construction and could be replaced by kinematic or combined kinematic-isotropic hardening rules. The most important problem, however, is the inelastic compressibility of C-C composites, which cannot be modeled by classical plasticity theories based upon J2 distorsional energy. In order to remove this difficulty, the use of the parabolic Mohr-Coulomb yield function is suggested. The Von Mises function $3J2 - \bar{\sigma}^2 = 0$ is replaced by $3J2 + \alpha\bar{\sigma}J1 - \bar{\sigma}^2 = 0$, where α is a parameter to be experimentally evaluated. This general yield surface is accurately representative of many materials which do not exhibit independence of hydrostatic stress and plastic incompressibility. Such yield functions are generally used in soil

or rock materials analyses with $\alpha>0$ (involving dilatancy); plastic compressibility requires validation analyses with $\alpha<0$.

Within the framework of studies about composite materials, Wu[8] also presents elliptic yield functions which account for tension and compression behavior differences. Nevertheless, such yield surfaces require an uneasy characterization and do not always have associated flow rules. An operational definition of models accounting for both plastic compressiblity and tension and compression behavior differences requires additional research.

Extensions of the model to "*n*D" reinforced C-C composites can be carried out without additional theoretical difficulties. This claim applies either to rod-reinforced C-C composites such as 3D materials wherein the reinforcements have fixed directions, or to materials reinforced with rods and yarns, which have an axisymmetric orthotropy and variable stiffening directions. The determination of a set of constitutive constants may be still more difficult and may require the direct use of the relation between homogenized monoaxial stiffness k, rod modulus E_r, and fiber volume fraction t as mentioned in Sec. III.C.

VI. Conclusions

The Sepcarb 4D material behaves as an elastic and orthotropic material up to 0.1% strain; beyond this value, the behavior of the composite appears to be elastoplastic. An appropriate three-dimensional finite element model accounting for these specifications has been developed. An isotropic elastoplastic constituent is superposed on four linear monoaxial stiffnesses which are equivalent, through homogenization, to an elastic and orthotropic constituent. The elastic constants of the model are evaluated through identification to the 4D orthotropic behavior in the low-strain range. In particular, the Young's modulus of the isotropic constituent appears to be directly determined using a compression test in the X direction of the 4D. The work-hardening data of the isotropic constituent are then conveniently evaluated using this X test.

The model defined in this way allows accurate prediction of the behavior of 4D specimens independent of the load orientation relative to the rod directions. The predicted and measured axial and radial displacements of 4D rings subjected to external pressure are also in reasonable agreement, indicating 1) the significant influence of the nonlinearities and 2) the adequacy of the model constants obtained from small-size specimen tests for the structural analysis of industrial-size 4D components. Improvements should still be obtained using more accurate plastic flow rules and considering isotropic elastic constants as matrix damage functions. This last improvement is particularly required to reduce unloading discrepancies between calculations and experimental data.

Appendix

The results are referred to a coordinate system wherein R is the first direction, the second and third directions being in the UY' plane defined in Fig. 10. The second direction is obtained from Y' by a rotation of angle θ around R. In such a Cartesian coordinate system, the 4D small strain elastic flexibility matrix is

$$H=\begin{bmatrix} A & B & B & 0 & 0 & 0 \\ B & C & D & -d & 0 & a \\ B & D & C & b & 0 & -a \\ 0 & -b & b & F & a & 0 \\ 0 & 0 & 0 & a & J & b \\ 0 & a & -a & 0 & b & F \end{bmatrix}$$

with

$$A=1/E_R \quad B=1/E_R-1/2G \quad C=1/E'$$

$$D=-2/3E+5/3E'-1/2G \quad F=4/3(1/E-1/E')+1/2G$$

$$J=2/3(1/E-1/E')+1/2G$$

These parameters are independent of θ; only a and b have angular variations around R:

$$a=(2\sqrt{2}/3)\cos\theta(\cos^2\theta-3\sin^2\theta)(1/E'-1/E)$$

$$b=(2\sqrt{2}/3)\sin\theta(\sin^2\theta-3\cos^2\theta)(1/E'-1/E)$$

References

[1] Maistre, M., "Development of a 4D Reinforced Carbon-Carbon Composite," AIAA Paper 76-607, July 1976.

[2] Lamicq, P., "Recent Improvements in 4D Carbon-Carbon Materials," AIAA Paper 77-822, July 1977.

[3] Geiler, D. E., "Thermostructural Analysis of Three-Dimensional Orthogonally Refinforced Carbon-Carbon Materials," *Proceedings of the 19th National Symposium of SAMPE,* April 1974, AD-783209, pp. 738-751.

[4] Pardoen, G. C., Falco, A. D., and Crose, J. D., "Asymmetric Stress Analysis of Axisymmetric Solids with Rectangularly Orthotropic Properties," *AIAA Journal,* Vol. 13, June 1975, pp. 756-761.

[5] Pardoen, G. C., "Asymmetric Stress Analysis of Axisymmetric Solids with Anisotropic Material Properties," *AIAA Journal,* Vol. 15, Oct. 1977, pp. 1498-1500.

[6] Marcal, P. V., "Finite Element Analysis with Material Nonlinearities—Theory and Practice," *Recent Advances in Matrix Methods of Structural Analysis and Design,* University of Alabama Press, 1971, pp. 257-282.

[7] Jones, R. M., "A Nonsymmetric Compliance Matrix Approach to Nonlinear Multimodulus Orthotropic Materials," *AIAA Journal,* Vol. 15, Oct. 1977, pp. 1436-1443.

[8] Wu, E. M., "Phenomenological Anisotropic Failure Criterion," *Composite Materials, Vol. 2, Mechanics of Composite Materials,* Chap. 9, edited by C. P. Sendeckyj, Academic Press, New York, 1974.